THEORETICAL AND EXPERIMENTAL ASSESSMENT OF THE OPTICAL RESPONSE OF PLANAR MICROLENS ARRAYS

BY

ERIK T. MISAWA

THESIS

Submitted in partial fulfillment of the requirements
for the degree of Master of Science in Mechanical Engineering
in the Graduate College of the
University of Illinois at Urbana-Champaign, 2011

Urbana, Illinois

Adviser:

Assistant Professor Kimani C. Toussaint, Jr.

ABSTRACT

The purpose of this thesis is to develop a theoretical method to estimate the optical properties and response of a homogenous, apposition microlens array. While other similar studies of microlens arrays have been performed, none were found to determine the total field of view, overlap in the field of view nor the estimated maximum resolution when using a broadband illumination source based on system parameters and spectral distribution of the input source. The necessary elements of optical theory and equations required for the derivation of the field of view parameters and broadband resolution are presented, including all the assumptions and constraints that were applied. The mathematical simulation model was implemented in MatLab and the simulated results are compared with experimental ones. Both results are shown to be accurate to within an acceptable factor. Finally, all MatLab code written for this thesis is included as attached m-files.

ACKNOWLEDGMENTS

I would like to take a moment and thank my adviser, Prof. Kimani C. Toussaint, Jr. who has given guidance, support, and provided me with a place to learn and grow for the past three years. A special thanks to Raghu Ambekar for helping me whenever I had questions, problems, wanted someone to bounce ideas off of, or just simply stuck in my research regardless of the time, day, or how busy he was. I would also like to thank Kaspar Ko, Brian Roxworthy, Santosh Tripathi, and the rest of the PROBE Lab for providing me assistance and friendship; you guys were my second family for the past few years and I appreciate it. Finally I would like to acknowledge my family (Eduardo, Sonia, and Richard Misawa) and my girlfriend, Miki Takagi. All of you gave me the motivation and were my moral support to keep pushing myself until the end.

TABLE OF CONTENTS

BACKGROUND

Over the span of millions of years, nature has forced organisms to evolve to become highly efficient in their energy use. For a certain species, if a particular mechanism will increase its chance of survival then that trait or mechanism will be passed on to the next generation. Classic examples would be of deep cave-dwelling animals where they live in complete darkness and have evolved to not have eyes. Another example includes certain species of chameleon that have the ability to change the color of their skin to help regulate their body temperature, aid in camouflage, and for social signaling. Many of these specialized mechanisms have direct similarities and application to man-made technologies. Instead of "reinventing the wheel", there is a field of study whose purpose is to artificially recreate these mechanisms.

Biomimetics is "the study of the formation, structure, or function of biologically produced substances and materials (as enzymes or silk) and biological mechanisms and processes (as protein synthesis or photosynthesis) especially for the purpose of synthesizing similar products by artificial mechanisms which mimic natural ones" [1]. An application of biomimetics is the artificial compound eye. Natural eyes are broadly classified in two types: the *single aperture eye* typically found in humans and other mammals, and the *compound eye* found in insects and crustaceans. A compound eye consists of a curved surface, almost hemispherical in shape, with several micro lenses arranged in an array. The actual number of micro lenses, also called lenslets, depends on the particular species ranging from the water fly which has a few hundred lenses, to worker bees which have a few thousand lenses, up to the Japanese dragon fly which has tens of thousands of micro lenses [2, 3]. The two main types of compound eyes are

the superposition compound eye and apposition compound eye. While both serve similar purposes, their working mechanisms differ greatly.

In the superposition eye, each photoreceptor's signal is a superposition of light from an array of lenslets so it is very light sensitive but spherical aberration are more significant since it is effectively a summation of each contributing lenslet's aberration [2]. Due to the superposition of light, each photoreceptor has a higher photon count compared to an apposition eye and so these eyes can be commonly found in nocturnal insects or in crustaceans that live in deep waters where there is lower lighting. An apposition eye has each lenslet matched to a photoreceptor allowing for fast visual processing but at a lower intensity contrast compared to a superposition compound eye [4]. In natural apposition compound eyes each optical channel – composed of the lenslet, photoreceptor, and channel between the microlens and photoreceptor -- is called an ommatidium. Between ommatidiums, pigments form opaque walls to prevent information entering a particular ommatidium to reach a photoreceptor belonging to a surrounding ommatidium and turn into a pseudo-superposition compound eye.

Since insects are significantly smaller than most mammals, their visual system are typically smaller in volume, require less processing power, and require less energy to construct and maintain than mammalian eyes [2]. Thus, for insects it would be a disadvantage to have single aperture eyes instead of compound eyes. Furthermore, compound eyes allow larger field of view, faster processing of visual information, better night vision, and in certain species, compound eyes allow the detection of different polarization states [5]. However, all this comes at the cost of having lower spatial resolution [5, 6].

While the characterization and fabrication of compound eyes have been extensively researched [7, 8], the application of artificial compound eyes has been slow due to difficulties arising from fabrication and large scale manufacturability [9]. As such, microlens arrays (MLA) have been used instead. A microlens array is a small sheet of glass with several lenslets arranged on the surface in a grid-like pattern. A microlens array is conceptually a planar compound eye and as such there exists both apposition and superposition microlens arrays (Figure 1); however because of the physical difference of a hemi-spherical dome versus a planer sheet there are some inherent differences in properties such as a smaller field of view. Microlens arrays can be found in applications ranging from adaptive optics for wavefront sensors, to solar concentrators [10], and to imaging including robot vision [11], and light field photography [12] and microscopy [13].

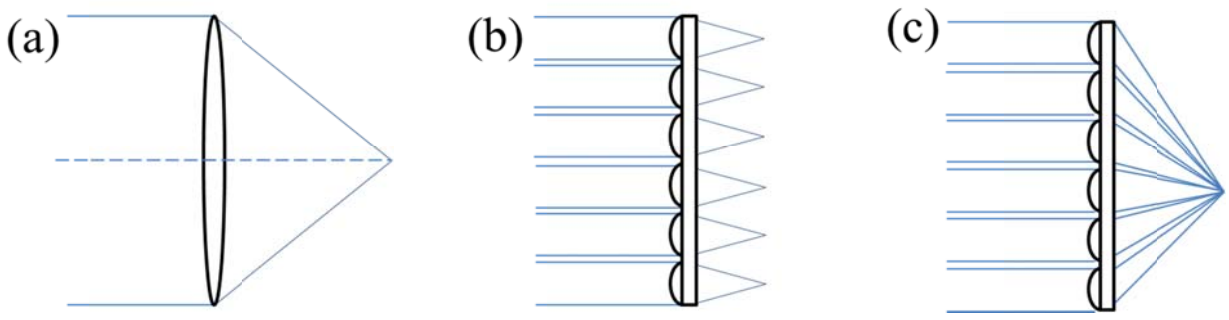

Figure 1: (a) Single aperture, (b) superposition, and (c) apposition microlens arrays.

While microlens arrays have been previously investigated for imaging applications, there are still opportunities for a multitude of novel applications to be explored. Microlens arrays are novel enough that at the beginning of 2011, only one major optical component company was

selling them. Therefore, microlens arrays need to be thoroughly characterized for next generation imaging techniques. The focus of this thesis will be on the theoretical and experimental assessment of the optical responses of microlens arrays. The goal of this study is to be able to estimate a microlens array's optical response based solely on its specifications and experimental setup parameters.

In the next chapter the theory needed to assess a microlens array's spatial resolution and field of view will be presented followed by simulation results. The following chapter will describe the experiment used to validate the estimated parameters from the simulations. This will include the experimental setup, calibration procedures and experimental results. The discussion chapter will compare the simulation with the experimental results and provide an assessment of predictive capabilities of the simulation model. Finally the references and appendix containing a copy of the MatLab simulations codes will conclude this thesis.

THEORY

OVERVIEW

In this chapter, the theory to determine the spatial resolution and field of view for an *N* x *M* microarray lens using a broadband light source will be presented. First, a brief overview of fundamental optics theory relevant to characterization and simulation of microlens arrays will be given. This will include the basics of imaging with a single-lens, and the concept of field of view and resolution for a monochromatic as well as a broadband source. The chapter concludes with simulation results for the resolution and field of view.

As mentioned in the previous chapter, a microlens array (MLA) is a homogenous array of several lenslets typically arranged in a square grid arrangement of lenslets but other geometries do exist [5, 14]. The lenses are commonly spherical or parabolic plano-convex lenses depending on whether it is a round or square aperture, respectively. The distance from one lens center to the adjacent lens center is known as the pitch (see Figure 2), which can be different from the diameter of the lens. Each lenslet produces its own unique image and each image does not overlap with adjacent images at the image plane. As a result, each individual lenslet can be modeled as a single-lens imaging system. Similarly, the resolution of microlens array will be the same as the resolution for an individual lenslet.

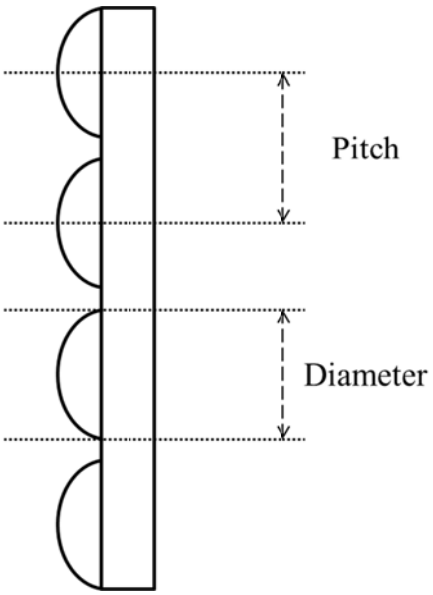

Figure 2: Diagram of a microlens array

There exist techniques to increase the effective field of view (FOV) and effective resolution of the microlens however they will not be used since they do not change the inherent characteristics of the microlens array itself but rather of the whole system. One such method is to place a pinhole array or another microlens array between the microlens array and image sensor. By "staggering" the second array relative to the microlens array, the field of view of each microlens is increasingly forced to point away from the central optical axis of the imaging system and so increasing the overall field of view of the whole system [2, 15, 16].

Another topic not covered in this thesis is extracting parallax information, also called 3D reconstruction [13]. The definition of parallax is the apparent displacement of an object from two or more different points of view [17]. In a MLA, each lenslet has its own point of view with respect to other lenslets so it is possible to extract several different 3D reconstructions from the same raw image [13]. In order to achieve the parallax phenomena, there must be overlap of the

input information between channels but not overlap of information between the signal of each channel, i.e. signal interference between channels.

SPATIAL RESOLUTION

Imaging

A single channel of a microlens array is defined as the lenslet, photoreceptor and the medium between the lenslet and the photoreceptor and the lenslets are the basic building elements of a microlens array. A channel can be modeled by a single-lens imaging system (Figure 3) and the thin lens imaging eq. (1)

$$\frac{1}{z_1} + \frac{1}{z_2} = \frac{1}{f}, \tag{1}$$

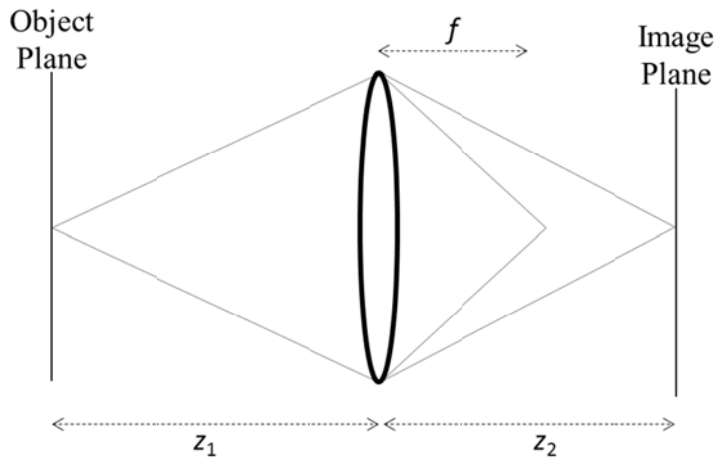

Figure 3: Single-lens imaging system

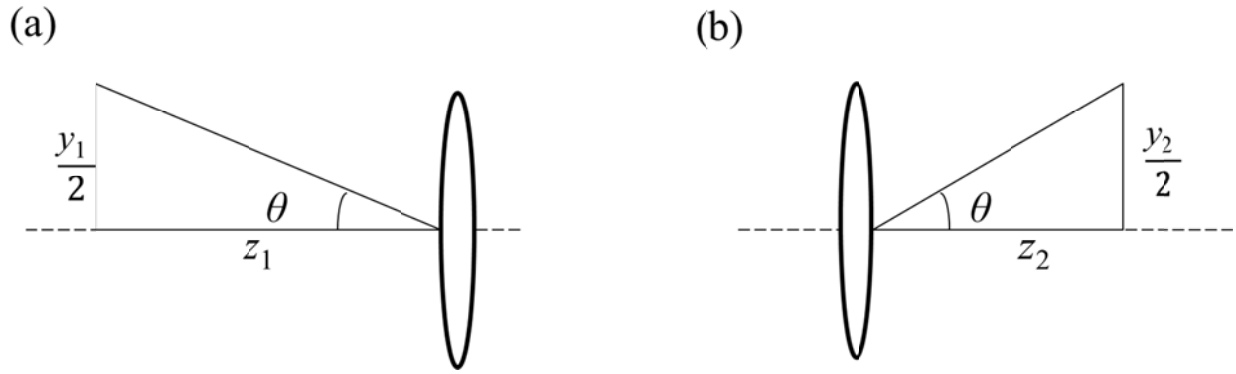

Figure 4: Additional imaging parameters. (a) Object plane to lens. (b) Lens to image plane.

where, z_1 is the distance from the target being imaged (object plane) to the lens, z_2 is the distance from the lens to the plane it is being imaged to (image plane), and f is the focal distance of the lens. In Figure 4, y_1 is the object size at the object plane and y_2 is the image size at the image plane. The angle θ can be determined and is the angle between the central optical axes to the top of the image on the image plane. The focal distance of the lens is a fixed parameter but the distances z_1 and z_2 can be changed and the ratio of z_2 / z_1 determines whether the image will be magnified or minified by the factor of their ratio. Therefore the object size, y_1, can be determined by the relationship given in eq. (3) which can be determined by setting the two versions of eq. (2) equal to themselves. If $z_1 = z_2$ then there will be no scaling of the object onto the image plane and this special case is called a "2-F imaging system".

$$\tan\theta = \frac{y_1}{2z_1} \quad or \quad \tan\theta = \frac{y_2}{2z_2} \tag{2}$$

$$\frac{y_1}{y_2} = \frac{z_1}{z_2} \quad or \quad \frac{y_1}{z_1} = \frac{y_2}{z_2} \tag{3}$$

Resolution

To calculate the maximum theoretical resolution of a single-lens, the resolution equation based on Rayleigh criterion can be used as given in eq. (4). The resolution is a function of the wavelength, λ, of the incoming light and the numerical aperture, *NA*, of the lens. In Figure 4, if the angle, θ, is smaller than 8^{o} then the small angle approximation can be used in solving for the *NA* of the lens, as shown in eq. (5), where *n* is the index of medium of propagation ($n \approx 1.0$ for air). Substituting eq. (2) into (5) gives eq. (6) which relates *NA* to lens and image parameters. Substituting eq. (6) into (4) results in the equation for resolution, given by eq. (7). It should be noted that this equation for maximum theoretical resolution is valid provided that the light source is a coherent, monochromatic beam.

$$Resolution = \frac{1.22\,\lambda}{NA} \tag{4}$$

$$NA = n\sin\theta \approx n\tan\theta \tag{5}$$

$$NA \approx \frac{ny_1}{2z_1} = \frac{ny_2}{2z_2} \tag{6}$$

$$Resolution \approx \frac{2.44\,\lambda\,z_1}{n\,y_1} = \frac{2.44\,\lambda\,z_2}{n\,y_2} \tag{7}$$

Modulation Transfer Function

The resolution can also be experimentally determined for real lenses. Given an optical setup, there are different methods and interpretations as to what is the smallest resolved feature.

One standard procedure to measure resolution is using the modulation transfer function (MTF). The formal definition of the MTF is:

$$MTF = \frac{\max(Intensity) - \min(Intensity)}{\max(Intensity) + \min(Intensity)} \tag{8}$$

For an optical system with no significant aberrations present, the MTF can also be modeled as in eq. (9) and (10) as a function of the NA and wavelength [18]. Here *v* is the frequency of the input in line pairs per millimeters.

$$MTF = \frac{2(\varphi - \cos\varphi \sin\varphi)}{n} \tag{9}$$

$$\varphi = \cos^{-1}\left(\frac{\lambda\, v}{2\, NA}\right) \tag{10}$$

In control systems theory, the modulation transfer function would be analogous to a swept sine wave analysis where a system's frequency response is characterized by recording the system's response to a swept sine input. Similarly, a modulation transfer function is the frequency response to a binarized swept sine input in the form of a target with lines of decreasing line pair spacing (Figure 5) or a target with sets of lines of varying gap spacing (Figure 6).

There are several definitions of cutoff frequency, and each definition leads to a different calculated resolution. One of the more common definitions for cutoff frequency and the one used in this study is the Rayleigh criterion which defines the cutoff frequency to be when the response decays to 25% (for incoherent illumination) of its maximum value, or approximately -3dB [19].

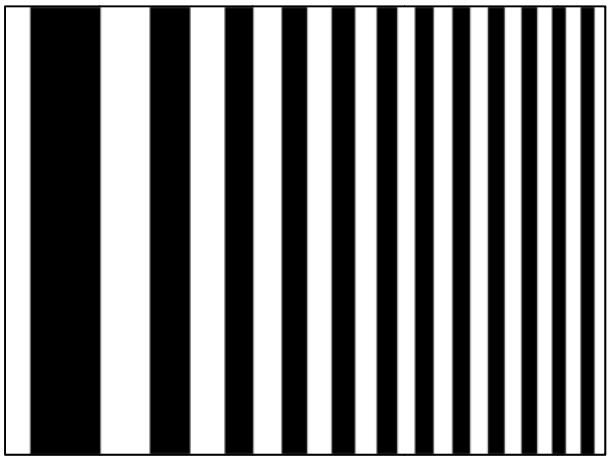

Figure 5: MatLab simulation of a varying spatial frequency, or "chirp", MTF target.

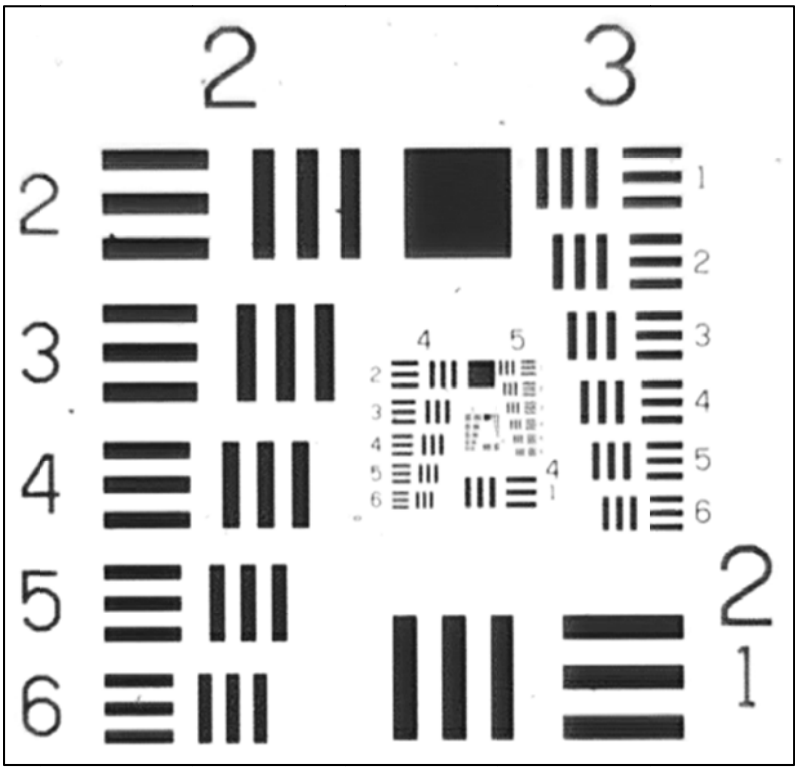

Figure 6: USAF 1951 resolution target.

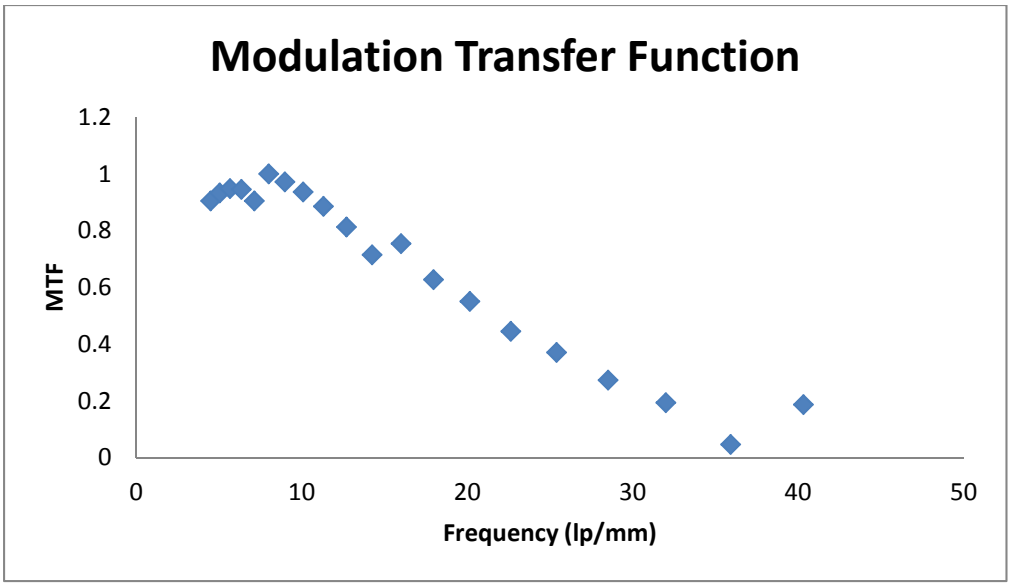

Figure 7: Example of a modulation transfer function for a USAF target similar to Figure 6. MTF of targets in groups 2, 3, 4 and 5.

Broadband Resolution

The equations for resolution, eq. (4) and therefore (7), depend on the wavelength of the input light. To determine the resolution with a broadband source (i.e. white light), the spectral distribution of the input light and the optical response of the system must be known for multiple wavelengths of the given spectrum. Subbarao [20] showed that the broadband resolution can be calculated using the optical transfer function (OTF) as shown in eq. (11) and (12)

$$O_B(\rho) = \frac{1}{A} \int_{-\infty}^{\infty} P(\lambda)\, O_S(\rho, \lambda)\, d\lambda \quad and \tag{11}$$

$$A = \int_{-\infty}^{\infty} P(\lambda)\ d\lambda \tag{12}$$

where O_B and O_S are the optical transfer functions of the system for a broadband and monochromatic source, respectively, and P is the spectrum for the broadband source. However,

these equations are for a continuous O_S and P, suggesting that an OTF exists continuously for every wavelength included in the spectral distribution. Since this is not possible, the discrete case is given in eq. (13) and (14) which can also be found in Subbarao's work [20]. Here it is assumed that the spectral distribution is negligible outside the range of λ_1 to λ_{m+1} and can be divided into m intervals where the distribution can be modeled as a linear function within each interval.

$$O_B(\rho) = \frac{1}{A} \sum_{i=1}^{m} \int_{\lambda_i}^{\lambda_{i+1}} P(\lambda)\, O_S(\rho, \lambda)\ d\lambda \tag{13}$$

$$A = \sum_{i=1}^{m} \int_{\lambda_i}^{\lambda_{i+1}} P(\lambda)\ d\lambda \tag{14}$$

In this thesis, the method used to characterize the optical response is the MTF and not the OTF so eq. (13) must be modified for the MTF of a broadband source (M_B) as a function of the MTF of a single wavelength (M_s). By definition of the OTF, the MTF is equal to the magnitude of the OTF, as shown in eq. (15) [21]. Also note that the spectral distribution, P, is positive for all values of λ such that A = |A|. Taking into account these two points, eq. (13) becomes eq. (16)

$$M(\rho, \lambda) = |O(\rho, \lambda)| \text{ and } \big(M(\rho, \lambda)\big)^2 = |O(\rho, \lambda)|^2 = \big(O(\rho, \lambda)\big)^2 \tag{15}$$

$$|O_B(\rho)| = \frac{1}{A} \left| \sum_{i=1}^{m} \int_{\lambda_{i+1}}^{\lambda_i} P(\lambda)\, O_S(\rho, \lambda)\ d\lambda \right| \tag{16}$$

$$|O_B(\rho)| \leq \frac{1}{A} \left(\sum_{i=1}^{m} \int_{\lambda_{i+1}}^{\lambda_i} |P(\lambda)|^2\, d\lambda \right)^{1/2} \left(\sum_{i=1}^{m} \int_{\lambda_{i+1}}^{\lambda_i} |O_S(\rho, \lambda)|^2\, d\lambda \right)^{1/2} \tag{17}$$

$$M_B(\rho) \leq \frac{1}{A}\left(\sum_{i=1}^{m}\int_{\lambda_{i+1}}^{\lambda_i}|P(\lambda)|^2\,d\lambda\right)^{1/2}\left(\sum_{i=1}^{m}\int_{\lambda_{i+1}}^{\lambda_i}|M_S(\rho,\lambda)|^2\,d\lambda\right)^{1/2} \quad (18)$$

Applying Hölder's inequality (specifically Schwarz's inequality) to eq. (16) results in eq. (17) and finally substituting the definition of OTF from eq. (15) to eq. (17) results in eq. (18). This equation estimates the theoretical MTF of a broadband light source as a function of the spectral distribution and the MTF at single wavelengths. It is important to note that this derivation of the broadband MTF is by definition the upper bound for the MTF. By definition of the Schwarz's inequality, the equality sign changed to represent the upper limit. Additionally, if eq. (9) and (10) are used to generate the monochromatic MTFs it was assumed that there is no significant aberration in the optical system but it has been shown in other works that aberrations are in fact present [2, 15] but not as significant compared to that of "bulk optics" [2]. Incorporating eq. (18) and (14) into MatLab is relatively simple assuming that the spectral distribution is known. The MTF of a single wavelength is calculated using eq. (9) and (10) and the trapezoidal rule is used for the numerical integration and summation involved in eq. (18). The code used for this simulation can be found in the appendix.

FIELD OF VIEW

Field of view (FOV) can be described as the angular or lateral extant of visual information. Assuming the optical setup presented in Figure 4, the angular field of view for that system will be equal to 2θ and is typically given in units of degrees. The lateral field of view, also called the "flat field of view" [19], for the same system would be equal to $2y_1$ and is given

as the lateral field of view (y_1) at an axial distance (z_1). In this thesis, FOV will be defined in terms of lateral distance.

The FOV of a single-lens system can be calculated with the assumption that the resulting image at the image plane cannot be larger than a length y_3 such that $y_2 \leq y_3$ (see Figure 4a, the need for this restriction will become apparent shortly). Given f, y_2, and z_2, then y_1 can be determined using eq. (1) and (2). To calculate the FOV of a MLA, recall that a MLA is simply an array of single-lens imaging systems. Therefore the method to determine the FOV of single-lens can be applied to the lenslets of the MLA.

Two adjacent microlenses will each produce its own individual image, however, if each sub-image is sufficiently wide then they will overlap with one another. To prevent crosstalk between optical channels, and thus rendering the apposition MLA into a quasi-superposition MLA, a constraint on the size of y_2 must be imposed that the image length will not be larger than the pitch must be observed (i.e. $y_2 \leq p$). To enforce this constraint, appropriate values for $z_1$and z_2 will be selected, so that the image is not excessively magnified. Conversely, if the sub-image is too small, then the MLA will not be used to its full potential as there will be unused pixels on the imaging sensor. An alternative method of controlling the image size is by manipulating the f-number with respect to the distance between the microlens and imaging plane [12] but this would require exchanging the MLA.

To achieve parallaxing there must be overlap in FOV; this creates a second constraint. To check for overlap, eq. (19) and (20) had to be derived to determine the validity of overlap for a given planar direction. If there is overlap, then the total lateral overlap is given by eq. (21) where N is the total number of microlens for the given lateral direction as the overlap. To

determine the total lateral field of view, eq. (22) was derived based from the geometry of the MLA as seen in Figure 8.

$$\text{If } y_1 \leq p \text{ , then no overlap exists.} \tag{19}$$

$$\text{If } y_1 > p \text{ , then overlap exists.} \tag{20}$$

$$\text{Total Overlap} = (y_1 - p)(N - 1) \tag{21}$$

$$\text{Total FOV} = y_1 + p(N - 1) \tag{22}$$

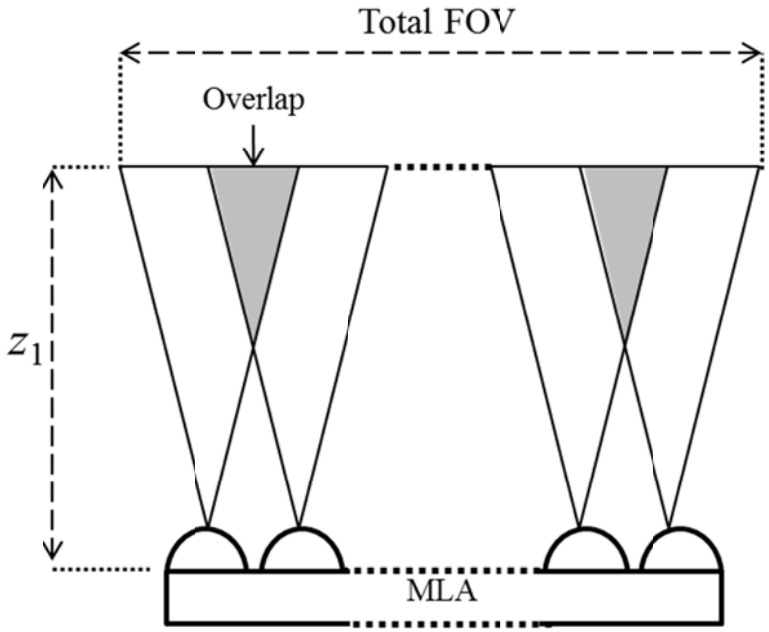

Figure 8: Diagram showing FOV and overlap.

The two conditions placed on the FOV are: size of y_2 must be imposed that the image length will not be larger than the pitch must be observed (i.e. $y_2 \leq p$) and to achieve parallax there must be overlap in FOV (i.e. $y_1 \geq p$). To simplify these two constraints, the only case where $y_1 = p$ and $y_2 = p$ is in a 2-f system which happens where there is no scaling between the image plane and the object plane. With this simplification the only situation where both constraints are satisfied and thus effectively reducing the constraints to one condition, is when the sub image is minimized, in other words, if $z_2/z_1<1$ then overlap and parallax exist.

SIMULATION RESULTS

To calculate all of the MLA parameters, the following input variables are needed as the minimum inputs set to carry out the calculation: the focal length of the MLA (f = 5.2 mm), pitch of the MLA (p = 150 μm), distance from the object plane to the MLA (z_1 = 24.89 mm), the sub-image size (y_2 = 0.079 mm), and the number of lenslets (N = 31). The values of these variables were chosen to match those in the experimental setup. From these variables, the remaining parameters were calculated:

- z2 = 6.57 mm
- y1 = 0.300 mm
- Magnification = 0.264
- FOV = 4.80 mm
- Overlap = 4.47 mm

The simulation results for the broadband spatial resolution simulation are given below. The inputs required for this simulation include the distance from the object plane to the MLA, the focal length of the MLA or the distance from the MLA to the image plane, the sub-image size, and the spectral distribution of the input light, seen in Figure 9 (values for these variables were determined from the FOV calculations above). The resulting MTF curve can be seen in Figure 10 and partial results can be seen in Table 1. Applying the Rayleigh criterion for resolution, the cutoff frequency corresponding to ~25% MTF is 22.64 lp/mm which corresponds to a lateral resolution of 22.08 μm.

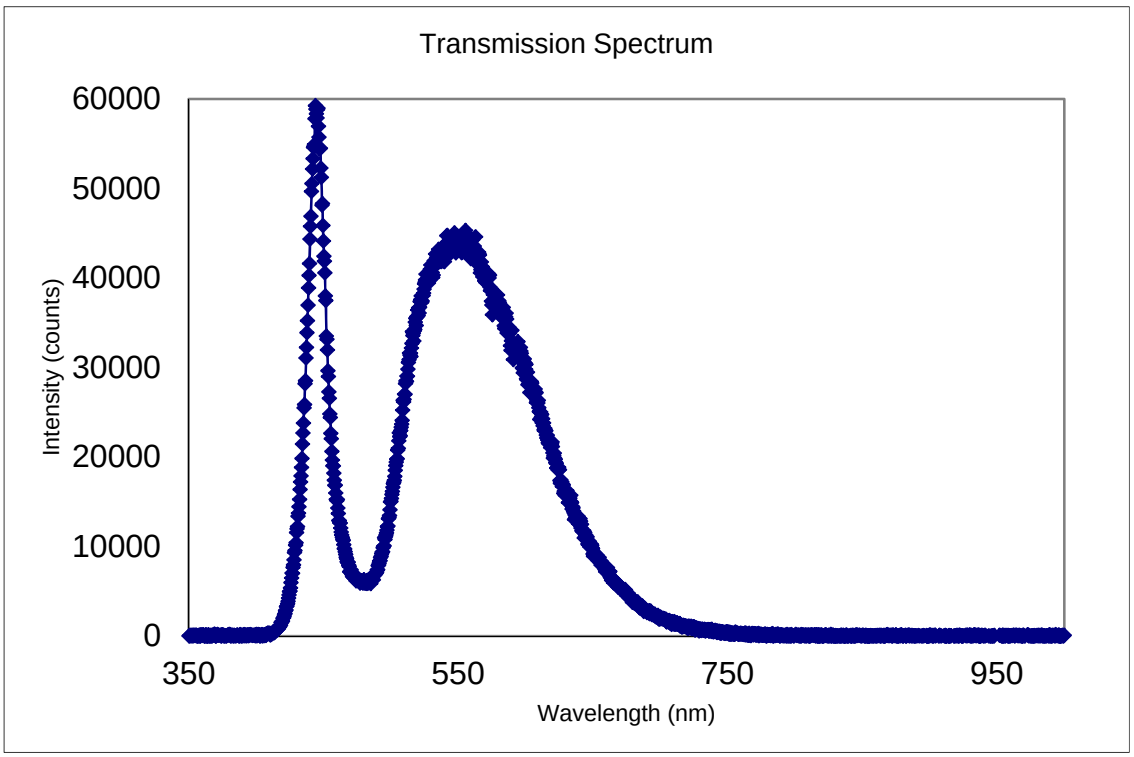

Figure 9: Spectral distribution of the LED flashlight used for the input source.

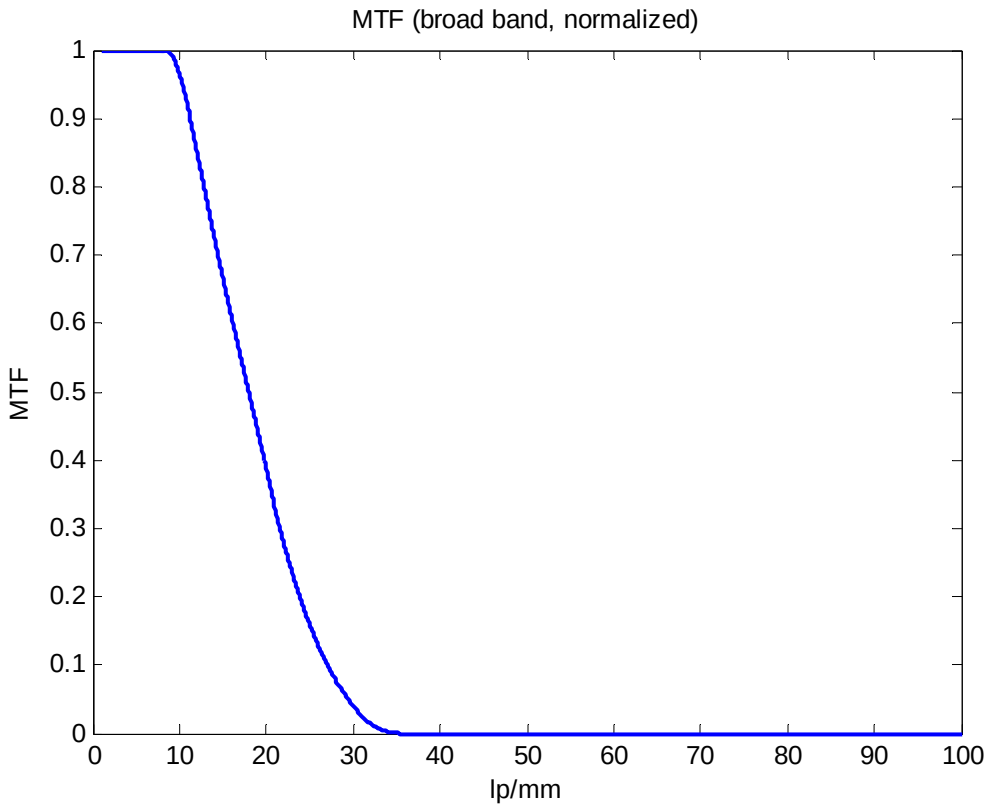

Figure 10: Broad band MTF curve.

Table 1: MTF simulation results.

%	% (actual)	lp/mm	µm
<100	99.9	8.62	58.0
75	74.9	13.7	36.6
50	50.2	17.9	27.9
30	30	21.6	23.2
25	25.1	22.6	22.1
20	20	23.9	21.0
10	9.91	27.1	18.5
5	5.04	29.4	17.0
4	4.04	30.0	16.7
3	3.05	30.7	16.3
2	1.96	31.6	15.8
1	1.01	32.6	15.3
0.1	0.100	34.5	14.5
0	0	35.4	14.1

EXPERIMENT

EXPERIMENTAL SETUP

A schematic for the experimental setup can be seen in Figure 11. A 633nm HeNe laser (Melles Griot, 25 LHR 151-249) is used to align all the optical components to a common optical axis and a LED flash light with a manual "focus" (SIPIK, SK68-3W) is used for illumination during the experiment. The "focus" adjusts the width of the beam and does not actually focus the beam to a point but this feature is used to adjust the light intensity. The two light sources are interchangeable via a flip mount located just past the output of the flashlight. There is a 4-*f* imaging system composed of two 50mm achromatic lenses (ThorLabs, AC254-050-B) relaying the object plane to the intermediate image plane. Located at a distance z_1 along the optical axis from the intermediate image plane is the microlens array (Thorlabs, MLA150-5C) and located a distance z_2 from the MLA is the CCD camera (Watec, WAT-902H Ultimate). Both the MLA and CCD camera are mounted on a linear stage (New Focus, 9067) to assist in focusing.

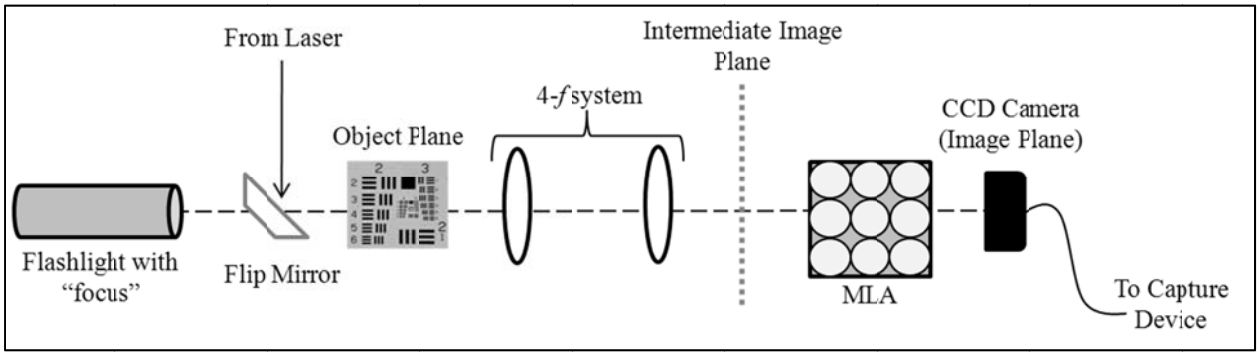

Figure 11: Experimental setup.

To determine the spectral distribution of the LED flashlight, the flashlight illuminated an optical fiber which was coupled to an Ocean Optics USB2000+ spectrometer. The resulting data, seen in Figure 9, was exported to a MatLab m-file to be used for the broadband resolution simulation discussed in the previous chapter.

This particular microlens array is made of fused silica (n~1.50) in a square grid arrangement of lenslets with a pitch of 150 μm. The lenslets are circular, plano-convex spherical lenses of diameter 146 μm and a focal length of 5.2 mm. The MLA is placed in a custom machined, 3mm thick aluminum mount with a 1 inch outer diameter so it can be placed in standard 1 inch optical mounts as well as in C- and CS-mounts. The MLA is 10 mm x 10 mm x 1.2 mm with approximately 66 x 66 micro lenses. However, the effective CCD image sensor is smaller than the MLA so not all lenslets will be imaged. The only parameter this will affect is the number of microlenses when calculating FOV.

Since the MLA has to be placed close to the CCD sensor due to the relatively small z_2 distance, the MLA had to be mounted inside the CS-mount tube and is held in place by a 2 mm thick retaining ring (Edmund Optics, NT58-70) on each side of a the MLA, see Figure 12. Currently, whenever the setup is changed the CS-mount has to be removed from the Watec main body and the retaining ring has to be rotated with a spanner wrench. The position of the retaining ring to the front of the CS-mount is then measured with a micrometer and added to the distance from the intermediate plane to the front of the CS-mount, resulting in z_1. Once the rear retaining ring is positioned, the MLA and front retaining ring are placed back and the CS-mount is placed inside the camera body. The reason the MLA is measured in this manner is because the CCD array of the camera is inaccessible and thus z_2 can never be directly measured. Due to this coarse mounting method, the positioning of the MLA is a very iterative and arduous task.

One important consideration when determining the experimental setup is the Nyquist sampling rate: the smallest resolved feature that the camera can resolve will be two times the size of the pixel cell. For that reason, it is important to design the experimental system such that the estimated resolution will be greater than the Nyquist limit.

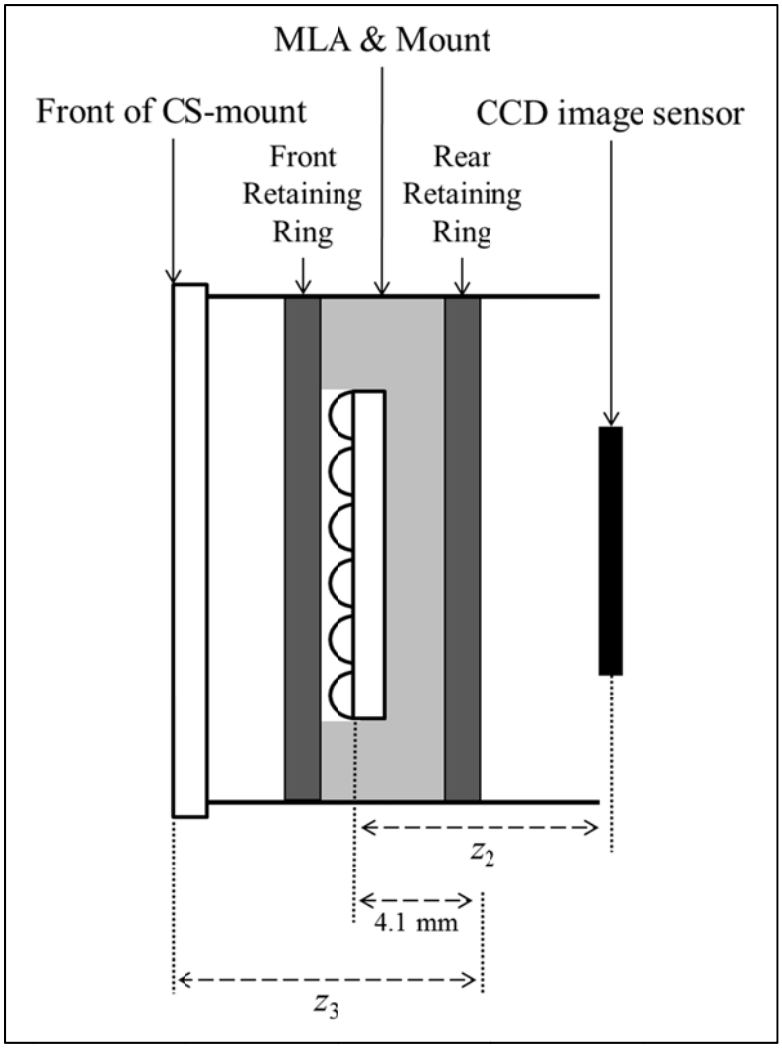

Figure 12: Diagram of the CCD CS-mount, MLA, and MLA mount

The calibration procedure of the MLA is as follows:

C.1) Place resolution target at the object plane

C.2) Mount the rear retaining ring and measure z_3 with a micrometer, see Figure 12, and adjust z_3 by adjusting the position of the retaining ring

C.3) Insert the MLA and mount, and the front retaining ring into the C-mount such that the MLA and mount sits flush with the rear retaining ring.

C.4) Place MLA/CCD system in experimental setup such that the distance from the conjugate object plane to the MLA is approximately the required z_1.

C.5) Repeat steps (C.2)-(C.7) until the measured z_1 matches the desired z_1.

C.6) The system will produce the sharpest image when it is in focus, or in other words when it satisfies the imaging equation, seen in eq. (1). So actuate the linear stage until the resulting image of the resolution target is in focus.

C.7) Measure the distance from the conjugate object plane to the front of CS-mount and add z_3 to this number. This is z_1. Use eq. (1) to calculate the actual z_2.

C.8) Compare to the desired z_2.

C.9) Remove the front retaining ring and MLA/mount and adjust z_3 accordingly.

C.10) Repeat steps (C.2)-(C.9) until z_2 is the desired length.

C.11) Remove the target from the object plane.

Field of View

Once the calibration has been completed, the first experiment is the FOV experiment. From this experiment, the remaining system parameters needed for the resolution experiment

will be calculated. As clarification, the spindle of a micrometer caliper is the cylindrical shaft that is actuated when the thimble is rotated. The anvil of a micrometer is the component that the spindle moves towards and if there is not object being measured, then the spindle would make contact with if fully actuated.

F.1) Starting with a calibrated system from previous calibration procedure, insert a micrometer caliper into the object plane and image the gap between the anvil and spindle.

F.2) Move and actuate the micrometer laterally until the gap created by the anvil and spindle only under-fill one set of MLA sub-images per side, see Figure 13 and Figure 14. Make note of the distance between the anvil and spindle as it will be the experimental value for the total FOV.

F.3) Save a picture of the resulting image from the CCD.

F.4) From the resulting image, count the number of microlens that are visible between the micrometer edges, see Figure 13, this will be N, the total number of lenslets.

F.5) Also from the resulting image, determine the diameter, in pixels, of each sub-image. Multiply the diameter by the actual width of each pixel in the CCD. This will be y_2.

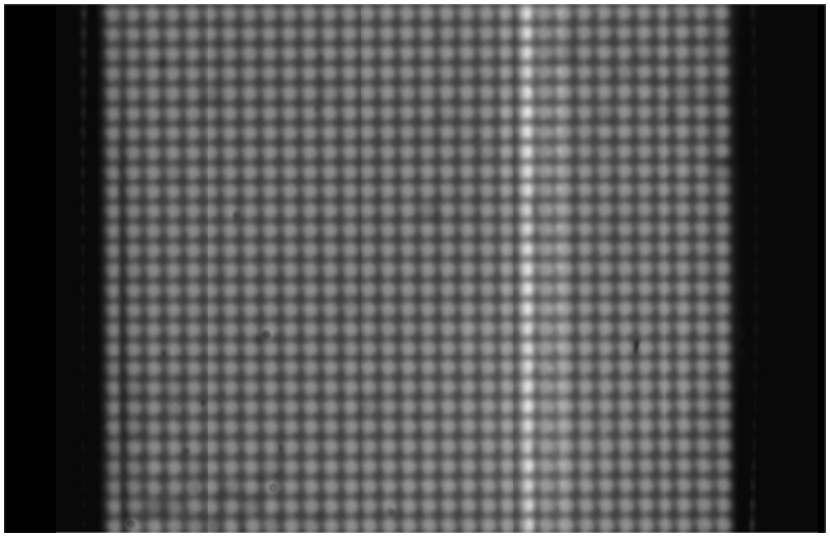

Figure 13: Resultant image from FOV calibration. Notice there is almost no under-fill of sub images from the anvil and spindle.

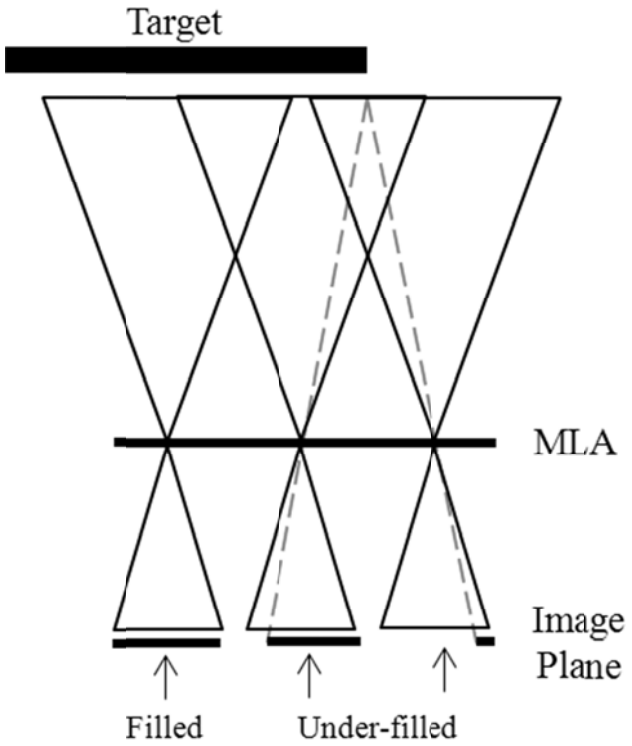

Figure 14: Diagram of under-filling lenslets.

From this calibration procedure, the total FOV, number of lenslets, and y_2 were determined. From the previous calibration procedure, z_1 was determined. From these, the total overlap and (calculated) total FOV can be estimated from eq. (21) and eq. (22) respectively. If the measured total FOV and the calculated total FOV are close, then the system is well calibrated.

Broadband Resolution

To experimentally calculate the resolution, one inserts a resolution target (Figure 15a) in the object plane of a calibrated MLA imaging system and records the resulting image. (For more information on resolution targets, please refer to the modulation transfer function section in the Theory chapter.) After the image has been recorded in a data file, it must be loaded into a software, such as MatLab, that is capable of converting the RGB data to intensity values.

To determine the MTF of an intensity image, one should focus on a specific line pair or a line set (Figure 15b) depending on whether the target is a chirped frequency resolution pattern or a USAF 1951 resolution target, respectively. The next step is to determine the maximum and minimum intensity for the line pair and apply eq. (8) to calculate the MTF (Figure 15c). This procedure is repeated for line pairs of increasing spatial frequencies to obtain a frequency response similar to Figure 7.

An MTF is typically given by percent contrast as a function of line pair per millimeter (lp/mm) where a line pair is defined as a black and white line pair. Once the cut off frequency, ω_c, has been determined it can be converted to resolution by eq. (23).

$$\text{Resolution} = \frac{1}{2}(\omega_c)^{-1} \tag{23}$$

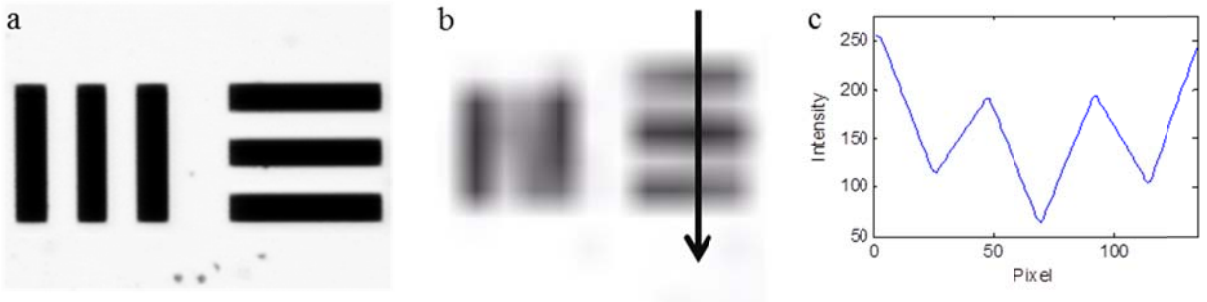

Figure 15: (a) Microscope image of a target from USAF resolution target. (b) MLA image of same target. Insert arrow represent location of line plot. (c) Line plot depicting the intensity distribution of the target. For this example, the MTF is approximately 0.50 (maximum intensity = 193, minimum intensity = 63.94).

EXPERIMENTAL RESULTS

The particular CCD camera used in this experiment is a Watec WAT-902H Ultimate and has rectangular pixels, 8.4 µm (H) x 9.8 µm (V), so resolution was determined for the horizontal orientation of the camera to optimize the lateral resolution. To make sure that the resolution would not exceed by the sensors' Nyquist limit, z_1 was tuned until the estimated cutoff frequency was lower than the Nyquist frequency limit. From calibration, z_1 was set to 24.9 mm resulting in an estimated cutoff of 22.6 lp/mm (22.1 µm resolution) compared to the Nyquist limit of 29.8 lp/mm (resolution of 16.8 µm). Additionally, from the FOV calibration, the FOV was measured to be 4.85 mm for N=31. Figure 16 is the image from the experimental setup and Table 2 shows the MTF values for targets close to the resolution limit. Again, the data closest to the Rayleigh's criterion (25% MTF) for the cutoff is highlighted.

Table 2: MTF experimental results.

Target	lp/mm	µm	MTF
3.3	10.1	49.5	0.373
3.4	11.3	44.2	0.338
3.5	12.7	39.4	0.268
3.6	14.3	35.0	0.274
4.1	16.0	31.3	0.176
4.2	17.95	27.9	0.155

Figure 16: Experimental image, refer to Figure 6 for specific target location.

DISCUSSION

In this chapter, the simulation results presented in the theory chapter and experimental results from the previous chapter will be compared and discussed, including potential sources for discrepancies. In this chapter, no new data will be introduced: all data and equations can be found in previous chapters.

Using eq. (22), the calculated FOV was 4.80 mm and from the FOV calibration, the actual FOV was 4.85 mm. This corresponds to an error of ~2%. Since the FOV depend on system parameters and can be determined geometrically from ray tracing, it is not surprising that the limiting factor would be the measurement accuracy. For example, when employing the FOV calibration procedure, it is extremely difficult to actuate the micrometer such that only one lenslet is under-filled.

When comparing the cutoff resolution from simulation (22.1 μm) with the experimental cutoff resolution (35.0 μm) it is apparent that the two sets of data are not identical. While the difference is approximately a factor of 1.6, it can be easily accounted for by spherical aberrations. The broadband resolution simulation effectively accounts for chromatic aberration, nonetheless it does not account for any spherical, coma, or field curvature aberration. These aberrations even can significantly affect quality research microscopes using infinity corrected objectives [22]. Furthermore, as shown in the theory chapter the derivation of the calculated resolution for the simulation, the resulting resolution will be an upper theoretical limit.

CONCLUSION

The aim of this thesis was to develop a method to estimate the optical properties of microlens arrays (MLA). The optical response of a homogenous MLA in an apposition configuration was studied. For an *N* x *M* MLA, the MLA can be considered as an array of single-lens imaging systems and modeled as such. Given the minimum input variables, it was shown that the total FOV and amount of overlap of the MLA can be estimated for each lateral direction assuming that overlap did exist. The conditions for when overlap exist was discussed and overlap exists only when the image is minified. Furthermore if the input source is a broadband source (i.e. white light) with a known spectral distribution, a method to determine the broadband MTF of the system, and thus the maximum achievable resolution for an aberration free system, was derived from a prior method implementing the OTF for a broadband source [20]. Experimentally the calculated FOV was shown to be correct to a high degree of confidence (~2% error) and that the estimated resolution was correct to within an acceptable factor due to spherical aberration and by the definition of the Schwarz's inequality. Additionally, calibration procedures for the experimental setup, FOV experiment, and resolution experiments were given.

Future work for this research project would include using a different camera to circumvent mounting issues with the MLA inside the camera tube Using a camera with an image sensor that is more accessible would reduce mounting issues arising from mounting the MLA between two retaining rings inside the CS-mount of the Watec camera. Additionally, deriving an alternate method to determine the broad band resolution that does not use the Schwarz's inequality would reduce the difference between the simulation and actual results as the Schwarz's inequality yields a very conservative maximum resolution. One future application of

the MLA would be to incorporate axicons as the lenslets in place of the plano-convex lenslets. Axicons are effectively a conical lens and can generate a Bessel-Gaussian beam which is an approximation of an ideal Bessel beam. Properties of Bessel beam is that is non-diffracting and the beam is capable of "self-healing": if a small obstruction is placed in the path of a Bessel beam, then the beam can reform behind the obstruction. Bessel beams have already been shown to produce multi particle (axially) optical traps [23] and MLA have already been used to produce a lateral array of potential wells at the focal plane, each capable of trapping [24], so combining the two to effectively from a three dimensional optical tweezer.

REFERENCES

1. biomimetics, in *Merriam-Webster Online Dictionary*. 2011, http://www.merriam-webster.com.
2. Duparre, J.W. and F.C. Wippermann, *Micro-optical artificial compound eyes.* Bioinspiration & Biomimetics, 2006. **1**(1): p. 1-16.
3. Jeong, K.-H., J. Kim, and L.P. Lee, *Biologically inspired artificial compound eyes.* Science, 2006. **312**(5773): p. 557-561.
4. Lee, L.P. and R. Szema, *Inspirations from Biological Optics for Advanced Photonic Systems.* Science, 2005. **310**(5751): p. 1148-1150.
5. Duparre, J., P. Schreiber, and R. Volkel. *Theoretical analysis of an artificial superposition compound eye for application in ultra flat digital image acquisition devices*. in *Optical Design and Engineering, September 30, 2003 - October 3, 2003*. 2004. St. Etienne, France: SPIE.
6. Bruckner, A., J. Duparre, and A. Brauer. *Advanced artificial compound-eye imaging systems*. in *MOEMS and Miniaturized Systems VII, 22 Jan. 2008*. 2008. USA: SPIE - The International Society for Optical Engineering.
7. Snyder, A.W., *ACUITY OF COMPOUND EYES - PHYSICAL LIMITATIONS AND DESIGN.* Journal of Comparative Physiology, 1977. **116**(2): p. 161-182.
8. Snyder, A.W., D.G. Stavenga, and S.B. Laughlin, *SPATIAL INFORMATION CAPACITY OF COMPOUND EYES.* Journal of Comparative Physiology, 1977. **116**(2): p. 183-207.
9. Popovic, Z.D., R.A. Sprague, and G.A.N. Connell, *TECHNIQUE FOR MONOLITHIC FABRICATION OF MICROLENS ARRAYS.* Applied Optics, 1988. **27**(7): p. 1281-1284.
10. Karp, J.H., E.J. Tremblay, and J.E. Ford, *Planar micro-optic solar concentrator.* Opt. Express, 2010. **18**(2): p. 1122-1133.
11. Franceschini, N., et al., *From Insect Vision to Robot Vision.* Philosophical Transactions of the Royal Society of London Series B-Biological Sciences, 1992. **337**(1281): p. 283-294.

12. R. Ng, M.L., M. Bredif, G. Duval, M. Horowitz, and P. Hanrahan., *Light Field Photography with a Hand-Held Plenoptic Camera.* Stanford University Computer Science Tech Report, 2005. **2005-02**.
13. Levoy, M., et al. *Light field microscopy*. in *ACM SIGGRAPH 2006 Papers, SIGGRAPH '06, July 30, 2006 - August 3, 2006*. 2006. Boston, MA, United states: Association for Computing Machinery.
14. Guo, F., H. Zhang, and K. Wang. *Point detection and positioning system of the target based on surface cluster eyes*. in *5th International Symposium on Advanced Optical Manufacturing and Testing Technologies: Optical Test and Measurement Technology and Equipment, April 26, 2010 - April 29, 2010*. 2010. Dalian, China: SPIE.
15. Tudela, R., et al. *An image restoration approach for artificial compound eyes*. 2008.
16. Fallah, H.R. and A. Karimzadeh, *MTF of compound eye.* Optics Express, 2010. **18**(12): p. 12304-12310.
17. parallax, in *Merriam-Webster Online Dictionary*. 2011, http://www.merriam-webster.com.
18. Kenneth R. Spring, M.W.D. *Modulation Transfer Function*. Nikon MicroscopyU 2010 [cited 2011; Available from: http://www.microscopyu.com/articles/optics/mtfintro.html.
19. Pawley, J.B., *Handbook of biological confocal microscopy*. 2006: Springer.
20. Subbarao, M., *Optical transfer function of a diffraction-limited system for polychromatic illumination.* Applied Optics, 1990. **29**(Copyright 1990, IEE): p. 554-8.
21. Williams, C.S. and O.A. Becklund, *Introduction to the optical transfer function*. 2002: SPIE Press.
22. Born, M., E. Wolf, and A.B. Bhatia, *Principles of Optics: Electromagnetic Theory of Propagation, Interference and Diffraction of Light*. 2000: Cambridge University Press.
23. Garces-Chavez, V., et al., *Optical levitation in a Bessel light beam.* Applied Physics Letters, 2004. **85**(Copyright 2004, IEE): p. 4001-3.
24. Sow, C.H., et al., *Multiple-spot optical tweezers created with microlens arrays fabricated by proton beam writing.* Applied Physics B: Lasers and Optics, 2004. **78**(Compendex): p. 705-709.

APPENDIX

The following simulations were written and conducted in Mathworks MatLab R2008a and R2010a on personal computers running Windows XP Professional SP3 (x86) and Windows 7 Professional (x64), respectively.

FOV TOOLKIT

This MatLab simulation of the FOV is a numerical implementation of eqns. (1), (3), and (19)-(22). By inputting the focal distance, the pitch, the (lateral) number of lenslets, z_1 or z_2, and the FOV, y_1 or y_2, the remaining parameters and total overlap are calculated.

Please see attached file: *MLAFOV.m* (File type: MatLab m-file)

MTF SIMULATION

This MatLab simulation of the broadband MTF implements eq. (18) in addition to a spectral distribution of the input source and other system parameters described under the "Simulation Results" in the Theory chapter. This simulation is designed to be ran independently of the FOV toolkit presented above.

Please see attached file: *bbMTF.m* (File type: MatLab m-file)